Non-linear charge-based battery storage optimization model with bi-variate cubic spline constraints

Per Aaslid [*,a,b], Frederik Geth [c], Magnus Korpås [b], Michael M Belsnes [a], Olav B Fosso [b]

[a] *SINTEF Energy Research, Trondheim, Norway*
[b] *Norwegian University of Science and Technology, Department of Electric Power Engineering, Trondheim, Norway*
[c] *CSIRO Energy Centre, Newcastle NSW, Australia*

A R T I C L E   I N F O

A B S T R A C T

Variable renewable generation demands increasing amount of flexible resources to balance the electric power system, and batteries stand out as a promising alternative. Battery models for optimization typically represent the battery with power and energy variables, while the voltage, current, charge variable space is used for simulation models. This paper proposes a non-linear battery storage optimization model in the voltage, current, charge variable space. The battery voltage is conceived as an empirical function of both state-of-charge and charge current and represented through bi-variate cubic splines. The voltage source converter losses are also approximated with a cubic spline function. Compared to energy-based storage models, the results show that this approach enables safe operation closer to the battery voltage and current limits. Furthermore, it prefers operating around high state-of-charge due to the higher efficiency in that region.

1. Introduction

1.1. Motivation and background

The increasing amount of variable renewable energy in the electric power system increases the demand of flexible resources and energy storage. Battery energy storage systems (BESS) are capable of delivering and consuming high power almost instantaneously, and BESS costs are decreasing rapidly. BESS is expected to play an important role in ensuring efficient and reliable operation of the electric power system. They are also easy to install and goes hand in hand with distributed power generation.

BESS installed in low voltage grids also have positive effects in medium and high-voltage grids [1]. Different applications of BESS systems are described in reference [2–4], such as energy trade, ancillary services and grid support, and customer energy management. The optimal strategy for BESS operation depend on the application, but the overall goal is to balance load and generation both in the time domain and geographically. Customer energy management is demonstrated in [5] where load is shifted due to grid tariff design in combination with PV. Energy trade is shown in [6] where the price differences over time is utilized for arbitrage, and a grid support application is shown in [7] where battery is applied for voltage control. Several applications are

often combined, such as simultaneous operation in day-ahead market (energy trade) and frequency reserve market (ancillary service) [8,9].

Batteries can be modelled both in the current, voltage, electric charge variable space, and in the power, energy variable space, hereby referred to as IVQ-model and PE-model respectively. The IVQ-model represents the battery state by counting charge in coulomb or ampere-hours, while the battery state for the PE-model is represented as energy in joule or watt-hours. The IVQ-model treats voltage and current as individual variables, while the PE-model is a special case of the IVQ-model with constant battery voltage. Since the battery voltage depends on both state of charge (SOC) and discharge current, the battery efficiency will also depend on those.

Existing battery simulation models span from simple models based on basic electric circuits to generic models with controlled voltage source [10]. One of the most common generic models is the Shepherd model [11], which has been further developed in [12,13]. All these models describe the battery behaviour in a more detailed and accurate way than the PE-models, and they provide insight into the battery voltage characteristics. However, an accurate model demands a complex model structure with many parameters, whereas a simpler model with fewer parameters will be less accurate.

Techno-economic BESS optimization models are dominated by PE-models [2,5,6,8,9]. In [14], an optimization model considering variations in efficiency for changing battery states is presented. Reference

---

Nomenclature

Sets and indices

t	Time step index
n / m	Degree of x / y in spline function
i / j	Spline function indices along x / y axis
x_i / y_j	Spline function control point at index i /j
tx_i / ty_j	Spline knot at index i / j

Parameters

ΔT_t	Step length at time t (h)
η^c / η^d	Battery charge/discharge efficiency
$\hat{p}_t^l$	Load forecast at time t (kW)
$\hat{p}_t^{PV}$	PV generation forecast at time t (kW)
c_t^p/c_t^s	Power purchase/sale price at time t (€ /kWh)
$E^{\min}$ / $E^{\max}$	Battery min/max storage energy (kWh)
$I^{b,ch}$ / $I^{b,dch}$	Battery max charge/discharge current (A)
$MC^{b,max}$	BESS marginal end-value at empty storage (€ /kWh)
N_{par}^b	Number of battery cells in parallel
N_{ser}^b	Number of battery cells in series
$P^{b,ch}$ / $P^{b,dch}$	Battery max charge/discharge power (kW)
$P^{p,max}$/$P^{s,max}$	Maximum purchase/sale (kW)
$P^{VSC,max}$	VSC maximum AC conversion power (kW)
$P_0^{VSC,loss}$/$P_2^{VSC,loss}$	VSC loss constant/quadratic term

$Q^{\min}$ / $Q^{\max}$	Battery min/max storage charge (Ah)
$V^{b,\ avg}$	Battery average voltage (V)
$V^{b,min}$ / $V^{b,max}$	Battery min/max operating voltage (V)

Variables and functions

$C_e(e)$	BESS energy end value function (€)
$C_q(q)$	BESS charge end value function (€)
e_t	BESS SOC (energy) at time t (kWh)
$f_v^b(q_t, i_t^b)$	Battery voltage function (V)
$f_{loss}^{VSC}(p_t^{VSC,AC})$	VSC loss function (kW)
i_t^b	Battery discharge current at time t (A)
$p_t^{b,ch}$ / $p_t^{b,ch}$	BESS charge/discharge power at time t (kW)
$p_t^{b,DC}$	DC discharge power from battery at time t (kW)
p_t^c/p_t^d	BESS PE-model charge/discharge power at time t (kW)
p_t^{PV} / $p_t^{PV,curt}$	PV generation and curtailment at time t (kW)
p_t^p/p_t^s	Power purchase/sale at time t (kW)
$p_t^{VSC,AC}$	Power from VSC to AC bus at time t (kW)
$p_t^{VSC,DC}$	Power to VSC from DC bus at time t (kW)
$p_t^{VSC,loss}$	VSC power loss at time t (kW)
q_t	BESS SOC (electric charge) at time t (Ah)
v_t^b	Battery voltage at time t (V)

---

[15] compares battery operation optimization including degradation with a PE-model, an equivalent circuit model and a single particle model, where the equivalent circuit- and the single particle model are IVQ-models. The single particle model combines detailed modelling, optimal operation and degradation well, but it requires a very detailed parametric description of the BESS.

Optimal BESS operation also relies on a accurate representation of power electronics. Many optimization models consider the battery and the voltage source converter (VSC) as a joint unit with a fixed charge and discharge efficiency. However, the VSC efficiency both depends on current and voltage. Reference [16] suggests the modelling of the VSC losses for optimization as a second order polynomial of current. The small scale VSC in [17] is provided with efficiency curves as a function of AC side power and DC side voltage. Detailed simulation of battery and power electronics is conducted in [18] showing that round-trip efficiency both depends on charge/discharge power and SOC, which is not accounted for in the PE-models.

1.2. Contributions and organization

The contribution of this paper is a non-linear IVQ-model for battery storage optimization. The battery voltage and the VSC power loss is embedded with cubic splines generated from empirical data of the battery voltage and the VSC efficiency. The cubic splines are implemented directly into the non-linear optimization problem. The model accounts for voltage and efficiency variations due to SOC and charge/discharge power, and efficiency variations in VSC. The battery voltage splines also encapsulate the battery series resistance. Moreover, since battery operation limitations are defined by voltage and current individually instead of power, this model enables safer operation close to the battery boundaries. Since the battery voltage is described by empirical data, it could also be updated based on measurement data as the battery degrades. Finally, the modelling method can easily be adapted to other battery types as well as other storage technologies such as hydrogen and hydro-power.

The remainder of this paper is organized as follows: Section 2 presents mathematical model of BESS, VSC, load, market and solar PV,

Section 3 presents numerical values used in this model, Section 4 presents results from numerical examples demonstrating the model capabilities, and Section 5 draws the conclusions and suggests further work.

2. Model description

This section presents an IVQ-model for a BESS, VSC, load and grid connection as shown in Fig. 1, where the objective is to minimize operation costs. Symbols used for the mathematical modelling are described in the nomenclature. A corresponding PE-model is also presented as a comparison to investigate the differences between the IVQ- and the PE-model.

2.1. Battery energy storage system

BESS are assembled by multiple chemical cells connected in series or parallel. This section will outline a non-linear IVQ-model, and a simple quadratic PE-model.

2.1.1. Assumptions

This paper studies battery operation for daily market optimization, typically 24–48 hours ahead. Therefore, self discharge and change in voltage characteristics due to degradation are neglected. Faster transients, which are more pronounced at high SOC [13], demanding time resolution down to a few seconds are also neglected. Wiring losses
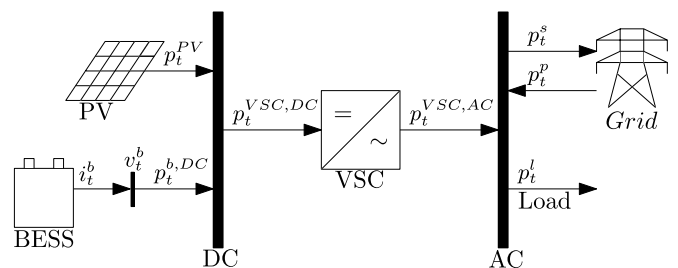

Fig. 1. Test system topology.

internal in battery and between VSC are much lower than other in-efficiencies and will not be accounted for.

2.1.2. PE-Model

A basic BESS optimization model is shown in (1), (2), (3), (4), (5), (6). The model assumes that the charge and discharge efficiencies are fixed. Numerical examples will later show the limitations of this assumption. This formulation often includes a charge/discharge complementarity constraint to prevent simultaneous charging and discharging. Since the system in this paper allows curtailing generation at no cost, this constraint has been excluded to avoid mixed integer variables.

$$e_t = \int_0^t \left(\eta_c p_t^c - \frac{1}{\eta_d} p_t^d \right) dt \tag{1}$$

$$P^{b,ch} = I^{b,ch} V^{b,avg} \tag{2}$$

$$P^{b,dch} = I^{b,dch} V^{b,avg} \tag{3}$$

$$E^{min} \leq e_t \leq E^{max} \tag{4}$$

$$0 \leq p_t^c \leq P^{b,ch} \tag{5}$$

$$0 \leq p_t^d \leq P^{b,dch} \tag{6}$$

2.1.3. IVQ-Model

A representation closer to the battery chemistry is considering the SOC in terms of charge q in ampere hours (7), and the voltage as a function of SOC and discharge current (8). Both values are given for an individual battery cell under the assumption that all battery cells will have identical SOC at all times. Equation (9), (10), (11) show the bounds for SOC, current and voltage respectively.

$$q_t = \int_0^t \left(-i_t^b \right) dt \tag{7}$$

$$v_t^b = f_v^b \left(q_t, i_t^b \right) \tag{8}$$

$$Q^{min} \leq q_t \leq Q^{max} \tag{9}$$

$$-I^{b,ch} \leq i_t^b \leq I^{b,dch} \tag{10}$$

$$V^{b,min} \leq v_t^b \leq V^{b,max} \tag{11}$$

2.1.4. Battery package

Let N_{ser}^b represent the number of cells in series and N_{par}^b the number of cells in parallel, hence the total number of cells is $N_{ser}^b \cdot N_{par}^b$. The battery discharge power is given by (12). The *DC* superscript is used to distinguish power on DC and AC side of the VSC.

$$p_t^{b,DC} = v_t^b \cdot N_{ser}^b \cdot i_t^b \cdot N_{par}^b \tag{12}$$

2.2. Voltage source converter

The voltage source converter (VSC) converts between DC and AC power in both directions. Typical DC sources and loads are battery storages and solar PV generations, but other DC loads and sources can also occur. The VSC is also subject to losses, and [16] suggests to model the losses with constant, linear and quadratic terms of the AC side current. For the PE-model, a convex relaxation with a constant and a quadratic term will be used to model VSC losses. For the IVQ-model, the losses are approximated with a cubic spline function.

2.2.1. Assumptions

The AC side is often part of a large utility grid with relatively stable voltage, hence the effects of voltage variation on this side are neglected. Moreover, the efficiency variations due to DC side voltage in [dataset] [17] are relatively small, hence they are neglected. Therefore, the losses will solely depend on the DC side power.

2.2.2. Model

The VSC efficiency is undefined when $p_t^{VSC,AC} = 0$ yielding a discontinuous function. Therefore, the power loss is expressed as the absolute power loss instead. The conversion from efficiency to absolute power loss is explained in Section 3.3. The IVQ-model uses a cubic spline function (13). The properties of cubic spline functions are discussed more in detail in Section 2.6, but the function shape will typically be close to quadratic. The PE-model uses a convex relaxation of a polynomial function (14). The VSC AC and DC power and losses for both models are tied together as shown in (15) where the losses always are positive.

$$p_t^{VSC,loss} = f_{loss}^{VSC} \left(p_t^{VSC,AC} \right) \tag{13}$$

$$p_t^{VSC,loss} \geq P_0^{VSC,loss} + P_2^{VSC,loss} \left(p_t^{VSC,AC} \right)^2 \tag{14}$$

$$p_t^{VSC,DC} = p_t^{VSC,AC} + p_t^{VSC,loss} \tag{15}$$

2.3. Load, generation and utility grid

The solar PV generation and load are given by separate forecasts. Generation curtailment and import from the power grid are decision variables.

2.3.1. Assumptions

To keep computational burden modest, uncertainties in forecasts are not accounted for. Generation can be curtailed, and power can be purchased from or sold to the utility grid at a fixed or variable exogenous positive price. In one of the examples, the effect of only being able to change the purchase/sale volume hourly will be studied. This aligns well with typical market structures where the energy is traded hourly either in the day-ahead or intra-day market. If forecast data has fewer data points than the optimization problem, data is re-sampled with linear interpolation.

2.3.2. Model

The relation between solar PV generation, forecast and curtailment is shown in (16).

$$\begin{aligned} p_t^{PV} &= \hat{p}_t^{PV} - p_t^{PV,curt} \\ p_t^{PV} &\geq 0 \end{aligned} \tag{16}$$

The PV generation is injected on the DC side, while the power exchanged with the utility grid is injected on the AC side. The PV and the BESS share a common VSC. Storing energy from utility grid yields larger losses than PV generation since power injected on the AC side must pass the VSC before being stored in the battery.

Utility grid imports and exports are permitted within certain limits as shown in (17).

$$\begin{aligned} 0 &\leq p_t^p \leq P^{p,max} \\ 0 &\leq p_t^s \leq P^{s,max} \end{aligned} \tag{17}$$

The resulting DC and AC bus power balances are shown in (18) and (19) respectively.

$$p_t^{VSC,DC} = p_t^{PV} + p_t^{b,DC} \tag{18}$$

$$\hat{p}_t^l = p_t^{VSC,AC} + p_t^{p,AC} - p_t^{s,AC} \tag{19}$$

2.4. Objective function

The objective function is given by the integral of the power exchange costs minus the BESS end storage value (20), which is described in Section 2.7.

$$\min \int_0^T \left(c_t^p p_t^p - c_t^s p_t^s \right) dt - C_q(q) \tag{20}$$

2.5. Integration rule

The integrals of (1), (7) and (20) can be discretized and solved numerically using methods for solving ordinary differential equations (ODE). Some of the simplest methods for solving the initial value problem in (21) are forward Euler (22), backward Euler (23) and the trapezoidal method (24).

$$y'(t) = f(t, y(t)), \; y(t_0) = y_0 \tag{21}$$

$$y_{n+1} = y_n + h \cdot f(t_n, y_n) \tag{22}$$

$$y_{n+1} = y_n + h \cdot f(t_{n+1}, y_{n+1}) \tag{23}$$

$$y_{n+1} = y_n + \frac{h}{2} \left(f(t_n, y_n) + f(t_{n+1}, y_{n+1}) \right) \tag{24}$$

The choice of method is of minor importance for the PE-model in (1) since the charging and discharging are independent of SOC. This paper has used forward Euler integration as shown in (25).

$$
\begin{aligned}
e_{t+1} &= e_t + \Delta T_t \left(\eta_c p_t^c - \frac{1}{\eta_d} p_t^d \right) \\
e_1 &= e_{init} \\
e_{end} &= e_T + \Delta T_T \left(\eta_c p_T^c - \frac{1}{\eta_d} p_T^d \right)
\end{aligned} \tag{25}
$$

However, in the IVQ-model the discharge power is function of voltage, while the voltage is a function both SOC and charge/discharge current. Hence, the choice of integration method will affect the results. Moreover, the choice of step length will also be more critical with respect to both the precision and the numerical stability.

The IVQ-model in (7) can be written recursively (26). Applying the different integration methods on (26) yields sets of sparse difference equations: the storage balance for forward Euler (27), backward Euler (28) and trapezoidal (29).

$$q_{t+1} = q_t + \int_t^{t+1} \left(-i_t^b \right) dt \tag{26}$$

Forward Euler:

$$
\begin{aligned}
q_{t+1} &= q_t - \Delta T_t i_t \\
q_1 &= q_{init} \\
q_{end} &= q_T - \Delta T_T i_T
\end{aligned} \tag{27}
$$

Backward Euler:

$$
\begin{aligned}
q_{t+1} &= q_t - \Delta T_t i_{t+1} \\
q_1 &= q_{init} - \Delta T_1 i_1 \\
q_{end} &= q_T
\end{aligned} \tag{28}
$$

Trapezoidal method:

$$
\begin{aligned}
q_{t+1} &= q_t - \frac{\Delta T_t}{2} (i_t + i_{t+1}) \\
q_1 &= q_{init} - \frac{\Delta T_1}{2} i_1 \\
q_{end} &= q_T - \frac{\Delta T_T i_T}{2}
\end{aligned} \tag{29}
$$

Forward integration rewards discharge using high power since the high voltage at high SOC yields higher power per charge unit, and the SOC update is delayed due to forward integration. Likewise, it will also reward charging using high power, as less power is demanded per ampere hour stored compared to low voltage charging. On the other hand, backward Euler gives incentive to discharge with lower power as the SOC is changed in advance. For these reasons, the trapezoidal method yields the most accurate integration for continuous operation, but will also build a slightly denser system of equations as the storage balance equations contain two discharge variables instead of one. The objective function is integrated in the same manner as the storage.

Overall, the presented approaches convert the ODE-constraints into a set of sparse difference equations (algebraic) of the same variables, which are only defined at a pre-determined set of time steps. These final sets of algebraic equations are used in the implementation of the optimization model, enabled by the use of non-linear programming solvers. Implementation and solution method are presented in Section 4.1.

2.6. Cubic splines

The constraints (8) and (13) will be modelled with cubic splines as these are compatible with non-linear programming, and possible to implement in interior point solvers. Interior point solvers are also relatively efficient at solving large-scale non-linear dynamic problems [19].

A spline function is a piece-wise polynomial function. A k degree spline function has continuous derivatives up to order $k - 1$, hence a spline function with degree 3 is guaranteed to have continuous derivatives up to order two. This is a necessary property for non-linear optimization tools requiring twice continuously differentiable functions. Spline functions are composed of multiple Bezier curves shown in (30). The Bezier curves are linear combinations of the Bernstein basis polynomials shown in (31) where n is the degree, and β_ν are known as Bernstein or Bezier coefficients.

$$BZ_n(x) = \sum_{\nu=0}^n = \beta_\nu be_{\nu,n}(x) \tag{30}$$

$$
\begin{aligned}
be_{\nu,n}(x) &= \binom{n}{\nu} x^\nu (1-x)^{n-\nu}, \\
\nu &= 0, \cdots, n, \; x = [0, 1]
\end{aligned} \tag{31}
$$

A property of the Bezier curve is that the start and the end value of the function is a linear combination of the Bezier coefficients, and the same applies for the start and the end values for the derivatives of the curve. This makes them well suited for building piece-wise polynomial functions with continuous derivatives.

A spline function can be uniquely described as a linear combination of basis functions as shown in (32), and this representation is known as B-splines. The spline function parameters are the control points x_i and knots t_i. The knots represent the distance between the control points. A k degree spline with $n + 1$ control points will consist of $n - k + 1$ polynomial segments. The basis function is constructed in a recursive manner using the Cox-de Boor formula (33)[20]. The derivatives are also defined as a linear combination of the basis functions.

$$S_{n,t}(x) = \sum_i \alpha_i B_{i,n}(x) \tag{32}$$

$$
\begin{aligned}
B_{i,0} &= \begin{cases} 1 \text{ if } t_i \le x \le t_{i+1} \\ 0 \text{ otherwise} \end{cases} \\
B_{i,k}(x) &= \frac{x - t_i}{t_{i+k} - t_i} B_{i,k-1}(x) + \frac{t_{i+k+1} - x}{t_{i+k+1} - t_{i+1}} B_{i+1,k-1}(x)
\end{aligned} \tag{33}
$$

Moreover, the bi-variate spline function is given by (34) where n and m are the spline degrees of the two dimensions x and y respectively. The bi-variate spline describes a smooth surface given by a mesh of control points α_{ij} where the corresponding knots are tx_i, ty_i.

$$S_{n,m,tx,ty}(x,y) = \sum_i \sum_j \alpha_{ij} B_{i,n}(x) B_{j,m}(y) \qquad (34)$$

Alternatively, the splines can also be described as a matrix of polynomials. This description is more extensive than the combination of basis splines, but the resulting function is differentiable in Julia/JuMP. Surface (*i, j*) of the bi-variate spline function on polynomial form is shown in (35).

$$
\begin{aligned}
S_{i,j,n,m,tx,ty}(x,y) &= \sum_{kn=0}^{n} \sum_{km=0}^{m} \beta_{i,j,kn,km} \; \Delta x_i^{kn} \; \Delta y_j^{km} \\
\Delta x_i &= x - x_i \\
\Delta y_i &= y - y_i
\end{aligned}
\qquad (35)
$$

Each polynomial surface is defined by $(n+1)\cdot(m+1)$ coefficients, for cubic splines in both x and y yields a 4 by 4 matrix with coefficients for each polynomial surface. These coefficients are obtained by evaluating (34) and its derivatives at the corners of the respective surfaces.

The splines have been generated using the Python Scipy [21] functions *bisplrep* and *splrep*, which are based on [20].

2.7. Battery energy storage system end value

In energy storage optimization, the storage tends to be emptied at the end of the optimization period, unless the end value is bounded by constraints, or the stored energy at the end is valuated in the objective function. A possible approach is to keep the end value fixed, for example to the initial value. However, the conversion between SOC in terms of charge and energy is not uniquely defined since the battery voltage depends on both SOC and charge/discharge current. Instead of keeping the end value fixed, an end value function is defined in this model. This enables comparison of the objective function through simulation of different cases even though the end point values are different. The valuation of end storage is a well established concept from hydro power scheduling [22,23], and [24] gives a general description also including PV generation.

When the SOC is 100%, it is unable to receive more power, hence the energy marginal value is zero. On the other hand, an empty storage is not capable of supplying energy, hence it has a high marginal value $MC_{\max}^b$. For simplicity, the marginal value of the end storage is set to vary linearly between these to points. The marginal value function for a PE-model is shown in (36). The corresponding storage end value function is the integral of (36) as shown in (37). The value function is converted from energy in the PE variable space *(kWh)* to charge in the IVQ variable space *(Ah)* through a conversion (38) under the assumption that the BESS is charged/discharged at constant voltage. The same conversion is used to convert the storage max value between PE and IVQ variable space. The resulting storage end value function is shown in (39).

$$MC_e(e_T) = MC^{b,max}\left(1 - \frac{e_T}{E^{b,max}}\right) \qquad (36)$$

$$
\begin{aligned}
C_e(e_T) &= \int_0^{e_T} MC_e(e)\, de \\
&= MC^{b,max}\left(e_T - \frac{e_T^{\,2}}{2E^{b,max}}\right)
\end{aligned}
\qquad (37)
$$

$$
\begin{aligned}
e_T &= V^{b,avg}\cdot N_{ser}^b\cdot N_{par}^b\cdot q_T \\
&= c_{eq}\cdot q_T
\end{aligned}
\qquad (38)
$$

$$C_q(q_T) = MC^{b,max}\cdot c_{eq}\left(q_T - \frac{q_T^{\,2}}{2\cdot Q^{b,max}}\right) \qquad (39)$$

2.8. Model summary

The objective and constraints of the PE-model and the IVQ-model are summarized in Table 1.

Table 1
Summary of PE- and IVQ-model equations.

PE-model	
Objective	(20), (37) and (38)
Storage constraints	(25)
Other constraints	(2) (3) (4) (5), (6), (14), (15), (16), (17), (18) and (19)

IVQ-model	
Objective	(20) and (39)
Storage constraints	(27), (28) or (29)
Other constraints	(8), (9), (10), (11), (12), (13) and (15), (16), (17), (18), (19)

The PE-model formulation is quadratic and convex. Note that simultaneous charging and discharging is possible to create artificial losses. In these situations, an equally good solution will be to curtail the generation.

The IVQ-model is continuous and twice differentiable, but the constraints are non-linear and non-convex. Ipopt searches for the optimal solution in an iterative manner, hence the spline functions are only evaluated at their current point for each iteration. Binary variables are therefore not needed to decide which segment of the spline function is active. However, the optimal solution is only local and can not be guaranteed to be the global optimum.

3. Case study data

This section presents numerical values used to describe the BESS and the VSC in the optimization problem, and the procedure for converting the data points into spline functions. The resulting BESS and VSC efficiencies are presented as well as the total system efficiency. Other general numerical values are presented in Table 2. Case-specific numerical results are presented in Section 4.
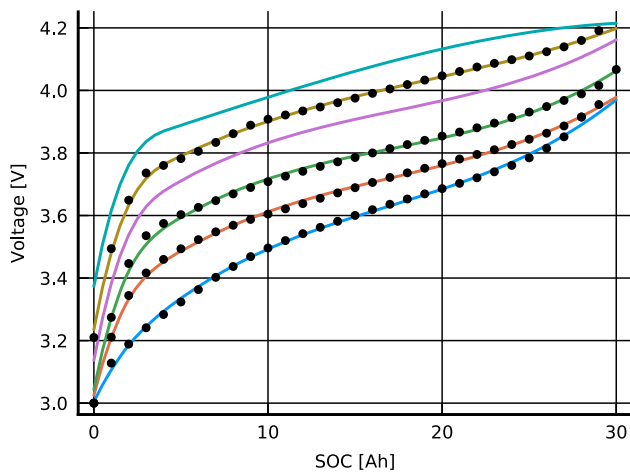
3.1. Battery voltage splines

The battery voltage is given by experimental values from a Nissan Leaf battery cell [dataset][25]. The cell has been charged at around 15 A and discharged at 30, 60 and 90 A while the voltage has been monitored. To generate the spline functions, the voltage has been sampled with uniformly distributed sample points in the SOC variable space q and for four selected charge/discharge currents yielding the bi-variate spline function $f_v^b(q_t, i_t^b)$. Fig. 2 shows the resulting splines compared to the original sampling points for different smoothing factors. In addition, voltage curves for 0 A and 30 A are shown to verify if the spline model predicts reasonable voltage values between and outside the sampling points. Fig. 2a shows that a low smoothing factor yields an accurate fit for the data points marked with black dots. However, the voltage at 0 A should be between the voltage at 15 A and -30 A which is not the case in Fig. 2a, hence is likely to be overfit. The intermediate smoothing factor in Fig. 2b fits quite well with the data point. The 0A voltage is also between the -30 A and the 15 A voltage, and the 30 A voltage seems to scale linearly compared to the other curves. However, the increasing slope for high SOC is not well captured for charging (positive current). The high

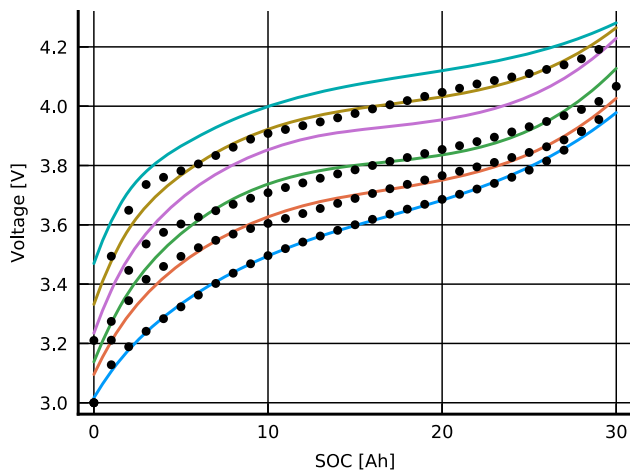**Table 2**
Model numerical values.

Battery & VSC	
$V^{\min}/V^{\max}/V^{avg}$	3.20/4.15/3.90 V
$Q^{b,min}/Q^{b,max}/Q^{init}$	0/29/20 Ah
$I^{b,ch}/I^{b,dch}$	30/90 A
$VSC^{\max}$	25 kW

Market	
$P^{p,max}/P^{s,max}$	10/10 kW
c^p/c^s	10/9 € /kWh
$MC^{b,max}$	15 € /kWh
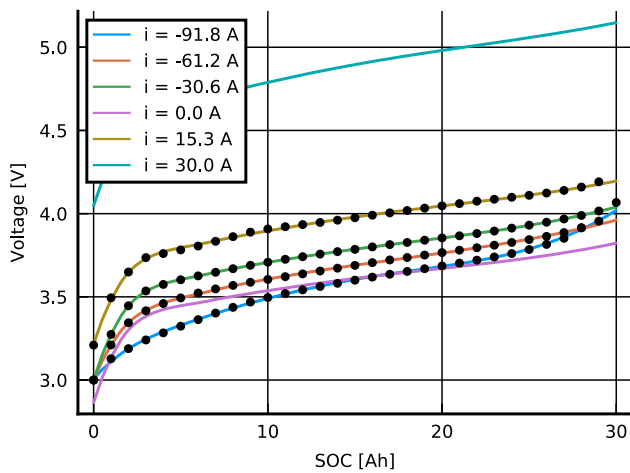
(a) Smoothing = 0.001

(b) Smoothing = 0.01

(c) Smoothing = 0.1

Fig. 2. Comparison of bi-variate spline curve and measured data for battery cell voltage for different smoothing factors.

smoothing factor in Fig. 2c captures the increasing slope for high SOC at the cost of accuracy, especially for low SOC where the deviation between the measured data points and the curves are significant. The intermediate smoothing factor 0.01 will be used further.

3.2. Battery modules and package

The Nissan Leaf 2013 battery package configuration consisting of 48 modules in series has been used. Each module has four cells, where two and two are in parallel. The experimental values in [25] has been obtained by cycling the battery cells between 3.0 V and 4.2 V. This configuration has $N_{ser}^b = 96$ and $N_{par}^b = 2$ yielding a voltage range from 288.0 to 403.2 V. Note that the examples in this paper use conservative voltage limits to illustrate the properties of the IVQ-model.

3.3. Voltage source converter loss curve

VSC loss values are obtained from [17] (SBS3.7–10), where the efficiency is given as function of AC side power. The efficiency is converted to absolute power loss as shown in (40), and the converted efficiency data points are used to generate the spline function $f_{loss}^{VSC}(p_t^{VSC,AC})$. To adapt the size of the VSC for the different cases, the $p_t^{VSC,AC}$ data points are scaled linearly with $P^{VSC,max}$ as the maximum value.
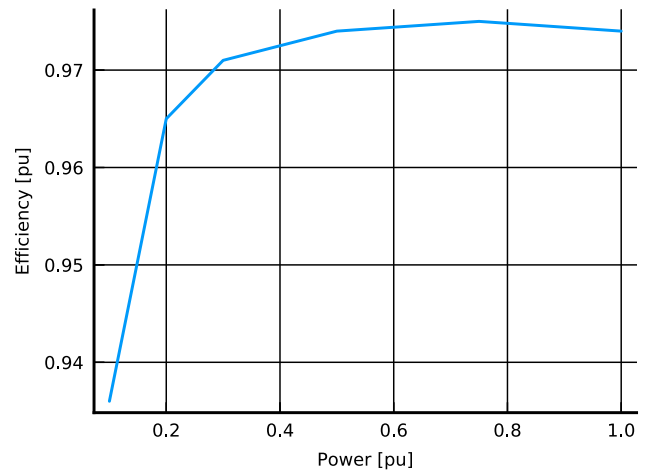
(a) Efficiency
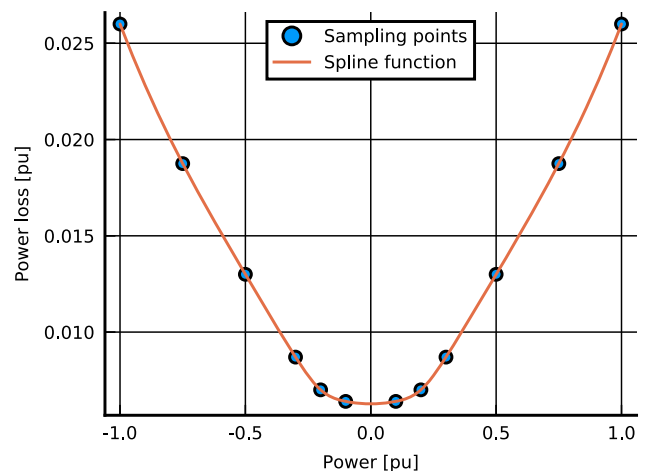
(b) Power loss

Fig. 3. VSC efficiency.

$$p_{loss}^{VSC}\left(p_t^{VSC,AC}\right) = \left(1 - \eta^{VSC}\left(p_t^{VSC,AC}\right)\right) \tag{40}$$

The VSC efficiency curve as function of per unit power is shown in Fig. 3a. This efficiency curve is for the nominal DC voltage 360 V. The VSC power loss sampling points and the resulting spline function are shown in Fig. 3b, where the solid line represents the spline function that is used in the optimization problem. The smoothing factor is 0.

The coefficients of the PE-model loss curve in (14) are fitted by evaluating the spline function for 0 and maximum power as shown in (41) and (42).

$$P_0^{VSC,loss} = f_{loss}^{VSC}(0) \tag{41}$$

$$P_2^{VSC,loss} = \frac{f_{loss}^{pu,VSC}\left(P^{VSC,max}\right) - P_0^{VSC,loss}}{\left(P^{VSC,max}\right)^2} \tag{42}$$

3.4. Battery and system efficiency

The battery round trip efficiency can be calculated based on the charge and discharge voltage. Assume the battery is charged at a constant current for a short optimization horizon, and then discharged with the same current. By neglecting the change in SOC due to the short time period, the battery round trip efficiency as a function of current and SOC can be found using (45). This has been mapped from the IVQ to the PE variable space, and the resulting numerical values are shown in Fig. 4a.

$$p^{b,dch} = f_v\left(q, i^b\right) \cdot i^b \tag{43}$$

$$p^{b,ch} = f_v\left(q, -i^b\right) \cdot i^b \tag{44}$$

$$\eta = \frac{p^{b,dch}}{p^{b,ch}} = \frac{f_v\left(q, i^b\right)}{f_v\left(q, -i^b\right)} \tag{45}$$

When storing energy in the battery, the energy can either come from surplus solar PV generation, or be purchased from the grid. Since PV generation is injected on the DC side, it does not have to pass VSC before it is discharged. However, when energy is purchased for storage, it is first converted to DC and then must be converted back later when consumed by the load. The system DC efficiency is the efficiency associated with storing solar PV energy for later use, and the VSC efficiency is multiplied with the BESS efficiency *once*. The AC efficiency is the efficiency when purchased energy is stored and consumed later, and the VSC efficiency is multiplied with the BESS efficiency *twice*. Both DC and AC efficiencies are shown in Fig. 4b and 4c respectively.

Both figures show that the system efficiency is highest for moderate power since the battery efficiency is highest for low power, while the VSC has a standby power consumption which shifts the system optimum. The efficiency decreases almost linearly when the SOC is around 50%, while the non-linearity is more pronounced for both high and low SOC.

4. Results and discussion

This section presents the implementation and solving method for the proposed models. Moreover, a simulation based validation method is proposed. Finally, the results from two examples are presented to demonstrate the capabilities of the IVQ optimization model. Both examples are built on the topology in Fig. 1 and the numerical values presented in Section 3, and solved using Ipopt in Julia/JuMP. The first example involves cycling of the battery, and demonstrates how the change in efficiency with respect to SOC influences the optimal solution. It also shows how the choice of step length and integration method can influence the accuracy of the numerical integration. The second case shows how the power delivery capability, due to voltage and current limits, is accounted for with an IVQ-model compared to a PE-model.
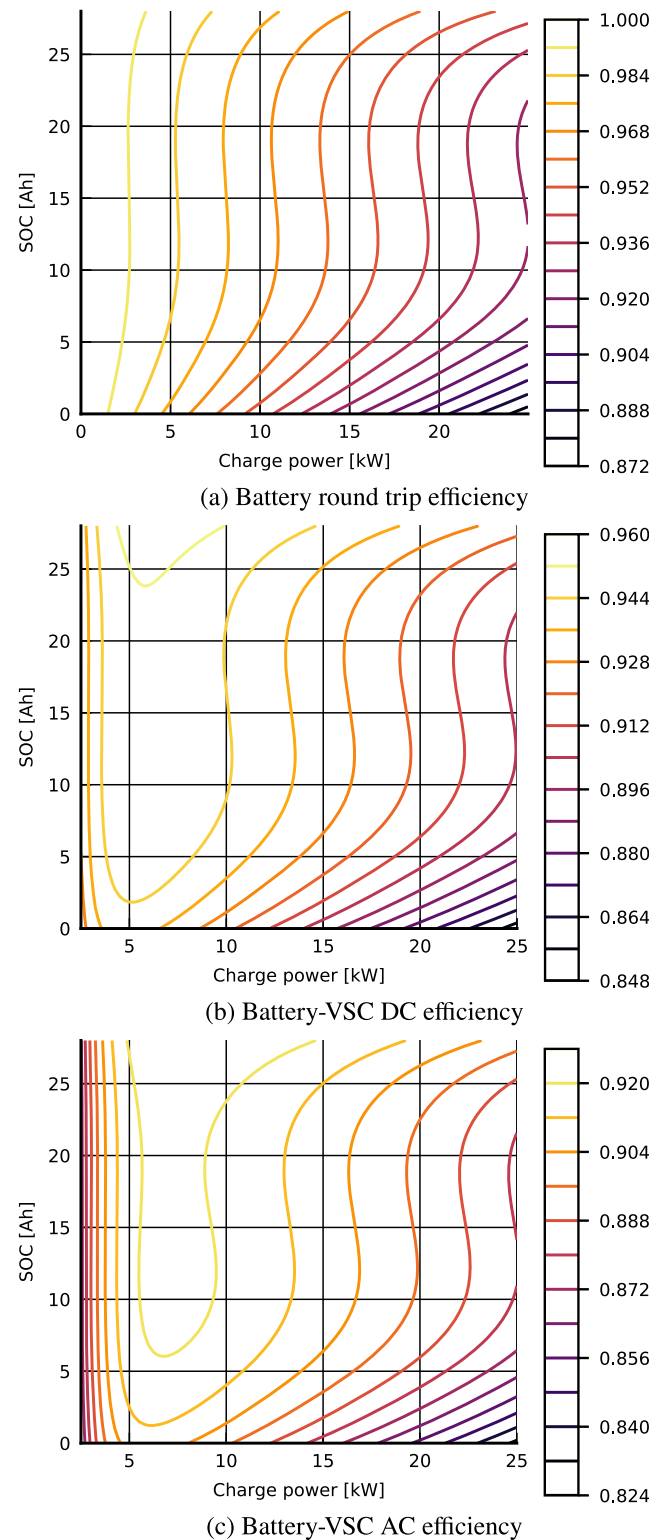

(a) Battery round trip efficiency

(b) Battery-VSC DC efficiency

(c) Battery-VSC AC efficiency

Fig. 4. Battery and VSC efficiencies.

4.1. Implementation and solution method

The problem is solved using the optimization toolbox JuMP (0.21.2) [26] in the programming language Julia (1.2) and the non-linear interior point solver Ipopt (3.12.10) [27]. Ipopt finds a local solution to non-linear and non-convex optimization problems where the objective and the constraint functions are twice continuously differentiable.

Computation time of Ipopt depends on problem structure as well as the underlying linear equality solver. Both the default solver in Ipopt, i. e. MUMPS, as well as the large scale solver PARDISO (6.0) [19] have been tested in this paper. PARDISO generally performs well on large scale systems [28].

Moreover, the voltage function and the VSC loss function must also be twice continuously differentiable. A common continuous function for describing this voltage is given by [12]. However, this function will often give a significant stationary offset compared to the actual voltage curve.

JuMP supports automatic differentiation of user-defined non-linear functions [26]. Instead of using a rigorously defined polynomial, the voltage surface and the VSC loss are described with a cubic spline function. The cubic spline function is piece-wise polynomial, but has continuous derivatives up to order two, hence no integer variables are needed to solve the problem. Since the voltage is a function of both i and q, a bi-variate cubic spline function is used to approximate (8), and a uni-variate cubic spline function is used to describe the VSC losses in (15).

4.2. Validation

To verify feasibility of the proposed schedules from the optimization models, a simulation model is used. The simulation model is based on the IVQ-model with forward Euler, but the step length is shorter, only 1 second. The simulation will therefore give a more accurate update of SOC under the assumption that the IVQ-model is the true model.

The simulation model assumes the load, grid exchange, VSC AC power and battery discharge is given by the optimization, and simulates the battery current and voltage, VSC loss, PV curtailment and SOC. This comparison identifies how much the SOC in optimization will drift of from the simulation result due to the inaccuracy in numerical integration. Since the PE-model does not include voltage and current as variables, the simulation is also used to check for voltage and current limit violations in the model result. Note that the SOC from optimization is used in this case since the effect of SOC drift should be kept apart from other effects. This simulation method ensures that the load is always met, and will reveal if the proposed schedule causes violation of current, voltage or SOC limits.

4.3. Optimality and integration method

The system efficiency depends on SOC, hence the optimal strategy involves operating around the optimal SOC as well as hitting the optimal end value. The relation between charge-discharge power and SOC depends on the integration method. To demonstrate this, the net load (load minus generation) is set to a sine wave with period 2 hours and amplitude 10 kW. The system is optimized for 36 hours which involves 18 charge/discharge cycles, which is long enough to let the battery cycling stabilize around the optimal SOC. Other numerical values of this test case are shown in Table 3

The case is optimized with step length 30, 10 and 1 min, and Fig. 5 shows the resulting optimized SOC, the simulation result and the optimization error (difference between optimization and simulation) at 10-minute optimization step lengths. Fig. 5a shows how the forward Euler cycles at lower SOC than the other methods, which is not optimal based on the efficiency surface shown in Figs. 4b, and 4c. The voltage at the beginning of a time step is used for integrating the SOC, hence for discharging the voltage will be higher than the actual voltage. The losses

Table 3
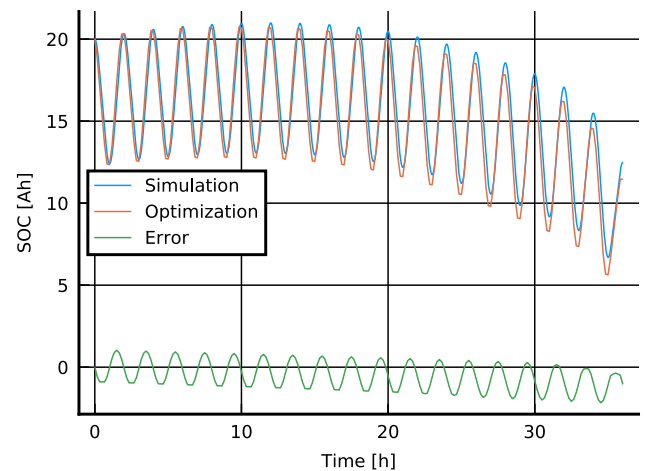Numerical values for sine wave case.

$p^{p,max}/p^{s,max}$	10.0/10.0 kW
c^p/c^s	10.0/9.0 €
$p^{VSC,max}$	25.0 € /kWh
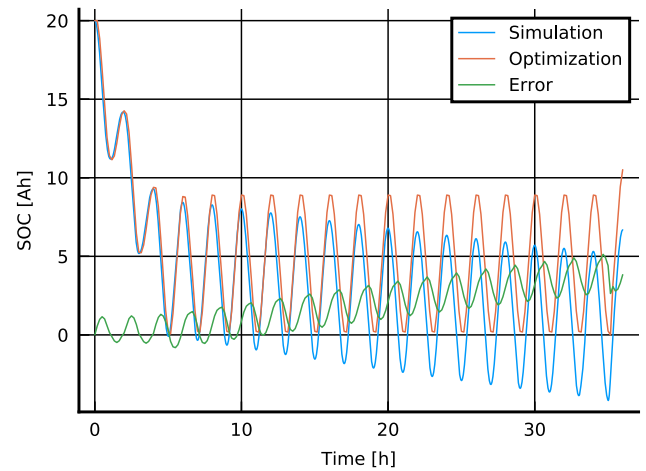
(a) Forward Euler
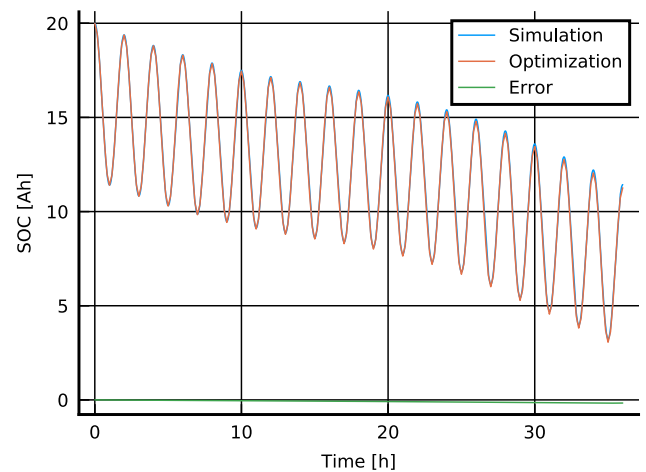
(b) Trapezoidal

(c) Backward Euler

Fig. 5. Comparison of optimization and simulation results for battery cycling with different integration methods with step length 10 minutes.

and the discharge current will therefore be underestimated and promote high discharge power. When charging, the voltage will be lower than the actual voltage, hence the charge current will be overestimated. In total, Fig. 5a shows that the simulated value drifts off from the optimized value and the error in SOC accumulated up to the value shown in Table 4. When the step size is reduced, the error is reduced significantly.

Table 5 summarizes number of variables and constraints for the

Table 4

Accumulated optimization error SOC (Ah) for different integration methods and step length with sine wave net load.

Step length	30 min	10 min	1 min
Forward	24.13	3.856	0.1222
Trapezoidal	−1.172	−0.1670	−0.003733
Backward	−2.950	−1.125	−0.1215

Table 5

Optimization statistics for different integration methods and step length with sine wave net load.

Step length		30 min	10 min	1 min
#Variables		1024	3040	30,256
#Equality constraints		733	2173	21,613
#Inequality constraints		74	218	2162
#Iterations	Forward	119	132	44
	Trapezoidal	46	39	50
	Backward	49	38	39
Solve time (s)	Forward	2.9	6.1	16.5
	Trapezoidal	1.6	2.0	20.0
	Backward	2.0	2.1	15.3

problems solved, and the respective computation time and number of iterations. The default linear solver in Ipopt, MUMPS, took between four and eight minutes solving the cases with one minute step length, and several of the other cases did not converge to the desired tolerance. Therefore, the PARDISO [19] solver was used instead, which gave a significant reduction in computation time for the largest cases and improved convergence tolerance.

For longer step lengths, forward Euler showed convergence problems for small initial storage values, which is in accordance with its known properties. This is also confirmed by the higher number of iterations needed for these cases in Table 5.

Fig. 5b and 5c show similar comparison for the trapezoidal method and backward Euler respectively. The trapezoidal method has a smaller error compared to the other methods, which is as expected, since the integration is based on the average voltage value for the time step. Backward Euler has a smaller deviation than forward Euler for the long time steps, while the error magnitude is almost identical for small step length. Backward Euler uses the voltage at the end of the time step to calculate the current, hence it will underestimate the needed charging current and overestimate the discharge current.

4.4. Solar PV smoothing

The numerical values for solar PV generation are acquired from [29], where the overcast series from *Varennes* with *overcast* cloud cover has
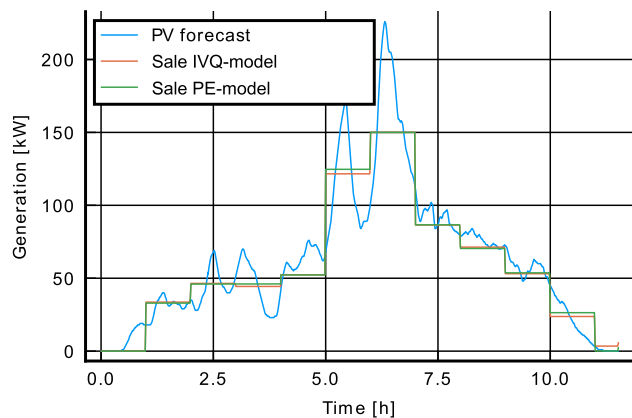
Table 6

Numerical values for PV smoothing case.

$P^{s,max}$	150.0 kW
c^{s}	10.0 € /kWh
$P^{VSC,max}$	150.0 kW

been used. The series have variable time resolution with step length ≤ 60s. This case demonstrates how the battery can be used to smooth the output from solar PV under the assumption that the system purchase/-sale only can be changed hourly. The PV generation is shown in Fig. 6 together with the system sale for both the IVQ- and the PE-model. Other numerical values specific for this case are shown in Table 6. It is noted that despite the differences, the dispatch curves are shaped similarly, suggesting that for the non-convex IVQ model the optimizer didn't converge to an obviously sub-optimal solution.

Fig. 7 shows the simulated SOC for the IVQ- and the PE-model, and the error between simulation and optimization. The result show that the PE-model violates the SOC lower bound (remark 1, indicated with a numbered red circle), and that the error increases when the battery is discharged at high power. The PE-model assumes constant battery efficiency, hence it does not capture the increasing loss for high discharge power causing the increase in error at remark 1.

The battery voltage is shown in Fig. 8a, and the both the upper and lower voltage is violated for the PE-model (remark 1–4). It would have been possible to adjust the power and energy limits such that they were not violated, but that would also put unnecessary conservative limits on the discharge power or SOC in other situations. Similar violations are observed for the current in Fig. 8b (remark 1).

Also note the difference is charging profile for the two models in Fig. 8c. Remark 1 and 2 shows how the charging is ramped down to avoid voltage limit violation, while at remark 3, the power is ramped up as the increasing battery voltage permits increasing charge power.

5. Conclusions

The IVQ optimization model enables operation closer to battery boundaries in terms of both voltage, current and SOC than a PE-model. Whereas a PE-model must implement conservative charge, discharge and SOC limits to ensure feasible solutions and battery life, the IVQ-model incorporates the voltage and current limits directly, allowing safe operation close to the battery limits. Moreover, the incorporation of the voltage surface and VSC efficiency with cubic splines enables the use of empirical data or updated measured data directly into the optimization model. The model can therefore be updated regularly through the battery lifetime providing optimal and feasible plans, even when the battery properties have changed due to degradation. Finally, the IVQ-model will ensure operation at the optimal SOC and charge/discharge
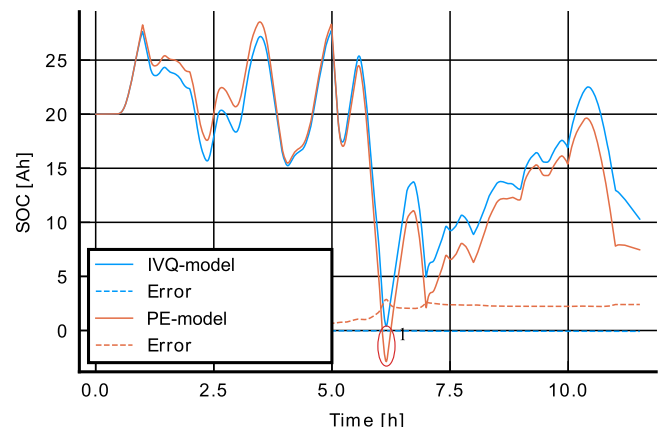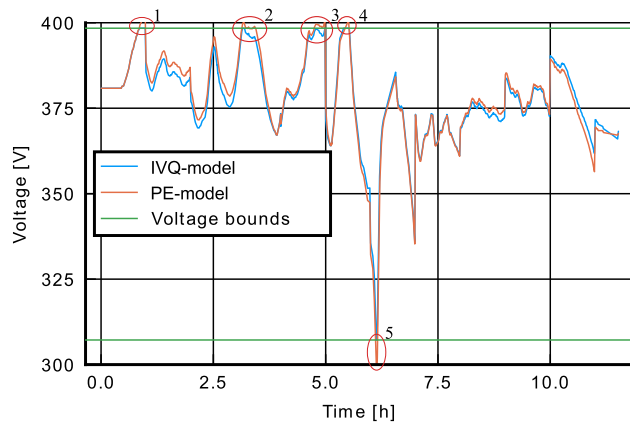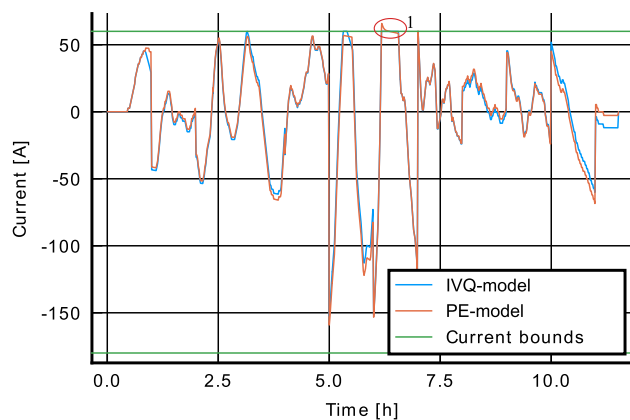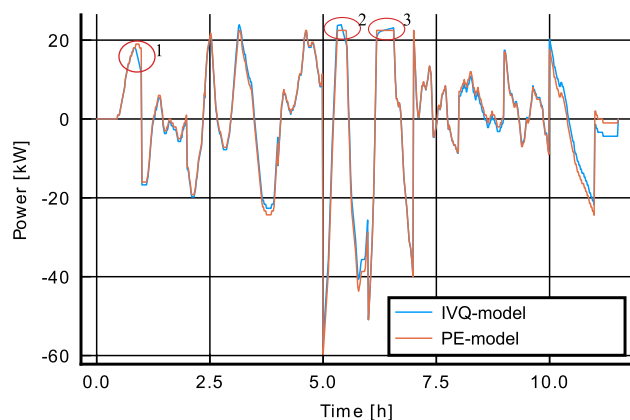

Fig. 6. PV generation and system output for PV smoothing case.

Fig. 7. Battery SOC for PV smoothing case.

(a) Battery voltage

(b) Battery charging current

(c) Battery charging power

Fig. 8. Battery voltage, current and power for PV smoothing case.

power yielding highest efficiency whenever possible. However, the results are sensitive to choice of numerical integration method and step length. The trapezoidal integration method has similar scalability to problem size as forward and backward Euler, but significantly less error for similar step lengths.

5.1. Further work

A possible extension of this model is to incorporate degradation costs associated with operative variables such as SOC and charge/discharge power. The modelling principle may also be adapted to other types of storage technologies such as hydrogen or hydropower.

Renewable generation is subject to uncertainty, and the error from

uncertainty is integrated over time when it comes to storage operation. Combining the proposed method with stochastic renewable generation and load is therefore also important further work.

Finally, the model may also be incorporated in an unbalanced OPF model using model predictive control to perform model-based congestion management through battery storage operation.

CRediT authorship contribution statement

Per Aaslid: Conceptualization, Methodology, Software, Formal analysis, Investigation, Visualization, Writing - original draft. **Frederik Geth:** Conceptualization, Methodology, Writing - review & editing. **Magnus Korpås:** Writing - review & editing. **Michael M Belsnes:** Writing - review & editing, Project administration. **Olav B Fosso:** Writing - review & editing, Supervision.

Declaration of Competing Interest

The authors declare that they have no known competing financial interests or personal relationships that could have appeared to influence the work reported in this paper.

Acknowlgedgments

References

[1] M. Müller, L. Viernstein, C.N. Truong, A. Eiting, H.C. Hesse, R. Witzmann, A. Jossen, Evaluation of grid-level adaptability for stationary battery energy storage system applications in Europe, Journal of Energy Storage 9 (2017) 1–11, https://doi.org/10.1016/j.est.2016.11.005.
[2] H.C. Hesse, M. Schimpe, D. Kucevic, A. Jossen, Lithium-ion battery storage for the grid - a review of stationary battery storage system design tailored for applications in modern power grids, Energies 10 (12) (2017) 2107, https://doi.org/10.3390/en10122107.
[3] O. Palizban, K. Kauhaniemi, Energy storage systems in modern grids-matrix of technologies and applications, Journal of Energy Storage 6 (2016) 248–259, https://doi.org/10.1016/j.est.2016.02.001.
[4] A. Castillo, D.F. Gayme, Grid-scale Energy Storage Applications in Renewable Energy Integration: A Survey, Energy Conversion and Management 87 (2014) 885–894, https://doi.org/10.1016/j.enconman.2014.07.063.
[5] A. Sani Hassan, L. Cipcigan, N. Jenkins, Optimal battery storage operation for PV systems with tariff incentives, Appl Energy 203 (2017) 422–441, https://doi.org/10.1016/j.apenergy.2017.06.043.
[6] B. Xu, A. Botterud, M. Korpas, Operational Valuation for Energy Storage Under Multi-stage Price Uncertainties, 2019.https://bolunxu.github.io/publication/xu_stochastic2019/http://arxiv.org/abs/1910.09149.
[7] J. Von Appen, T. Stetz, M. Braun, A. Schmiegel, Local voltage control strategies for PV storage systems in distribution grids, IEEE Trans Smart Grid 5 (2) (2014) 1002–1009, https://doi.org/10.1109/TSG.2013.2291116.
[8] M. Kazemi, H. Zareipour, N. Amjady, W.D. Rosehart, M. Ehsan, Operation scheduling of battery storage systems in joint energy and ancillary services markets, IEEE Trans. Sustainable Energy 8 (4) (2017) 1726–1735, https://doi.org/10.1109/TSTE.2017.2706563.
[9] X. Ai, Z. Wu, J. Hu, Y. Li, P. Hou, Robust operation strategy enabling a combined wind/battery power plant for providing energy and frequency ancillary services, International Journal of Electrical Power & Energy Systems 118 (2020) 105736, https://doi.org/10.1016/j.ijepes.2019.105736.
[10] S.M. Mousavi G., M. Nikdel, Various battery models for various simulation studies and applications, Renewable Sustainable Energy Rev. 32 (2014) 477–485, https://doi.org/10.1016/j.rser.2014.01.048.
[11] C.M. Shepherd, Design of primary and secondary cells - Part 2. An equation describing battery discharge. Journal of Electrochemical Society 112 (1965) 657–664.
[12] O. Tremblay, L.-A. Dessaint, A.-I. Dekkiche, A generic battery model for the dynamic simulation of hybrid electric vehicles. 2007 IEEE Vehicle Power and Propulsion Conference, IEEE, 2007, pp. 284–289, https://doi.org/10.1109/VPPC.2007.4544139.http://ieeexplore.ieee.org/document/4544139/.
[13] O. Tremblay, L.-A. Dessaint, Experimental Validation of a Battery Dynamic Model for EV Applications, World Electric Vehicle Journal 3 (2) (2009) 289–298, https://doi.org/10.3390/wevj3020289.http://www.mdpi.com/2032-6653/3/2/289.
[14] P. Fortenbacher, J.L. Mathieu, G. Andersson, Modeling and Optimal Operation of Distributed Battery Storage in Low Voltage Grids, IEEE Transactions on Power Systems 32 (6) (2017) 4340–4350, https://doi.org/10.1109/TPWRS.2017.2682339.http://ieeexplore.ieee.org/document/7879188/.

[15] J.M. Reniers, G. Mulder, S. Ober-Blöbaum, D.A. Howey, Improving optimal control of grid-connected lithium-ion batteries through more accurate battery and degradation modelling, Journal of Power Sources 379 (2018) 91–102, https://doi.org/10.1016/j.jpowsour.2018.01.004.https://www.sciencedirect.com/science/article/pii/S0378775318300041.

[16] H. Ergun, J. Dave, D. Van Hertem, F. Geth, Optimal power flow for AC-DC grids: formulation, convex relaxation, linear approximation, and implementation, IEEE Trans. Power Syst. 34 (4) (2019) 2980–2990, https://doi.org/10.1109/TPWRS.2019.2897835.

[17] SMA Solar Technology, Technical Information, Efficiency and Derating, Sunny Boy/Sunny Boy Storage/Sunny Tripower/Sunny Mini Central/Sunny Highpower, 2020.https://files.sma.de/dl/1348/WirkungDerat-TI-en-47.pdf.

[18] M. Schimpe, M. Naumann, N. Truong, H.C. Hesse, S. Santhanagopalan, A. Saxon, A. Jossen, Energy efficiency evaluation of a stationary lithium-ion battery container storage system via electro-thermal modeling and detailed component analysis, Appl Energy 210 (2018) 211–229, https://doi.org/10.1016/j.apenergy.2017.10.129.

[19] D. Kourounis, A. Fuchs, O. Schenk, Toward the next generation of multiperiod optimal power flow solvers, IEEE Trans. Power Syst. 33 (4) (2018) 4005–4014, https://doi.org/10.1109/TPWRS.2017.2789187.

[20] P. Dierckx, Curve and Surface Fitting with Splines., Oxford University Press, Inc., New York, 1995.https://books.google.com/books?hl=no&lr=&id=-RIQ3SR0sZMC&oi=fnd&pg=PR15&dq=Curve+and+Surface+Fitting+with+Splines&ots=IPSe_5k45a&sig=V9YUfX5SbtLVmGR8eb7Bak_bMG0.

[21] Yoshiki, S.C.V. Pauli, G. Ralf, O. Travis E., H. Matt, R. Tyler, C. David, B. Evgeni, P. Pearu, W. Warren, B. Jonathan, v.d.W. Stéfan J., B. Matthew, W. Joshua, M. K. Jarrod, M. Nikolay, SciPy 1.0: fundamental algorithms for scientific computing in Python, Nat. Methods 17 (3) (2020) 261–272, https://doi.org/10.1038/s41592-019-0686-2.

[22] O.B. Fosso, A. Gjelsvik, A. Haugstad, B. Mo, I. Wangensteen, Generation scheduling in a deregulated system. the norwegian case, IEEE Trans. Power Syst. 14 (1) (1999) 75–80, https://doi.org/10.1109/59.744487.

[23] O. Wolfgang, A. Haugstad, B. Mo, A. Gjelsvik, I. Wangensteen, G. Doorman, Hydro reservoir handling in Norway before and after deregulation, Energy 34 (10) (2009) 1642–1651, https://doi.org/10.1016/j.energy.2009.07.025.

[24] H.G. Svendsen, O.C. Spro, PowerGAMA: A new simplified modelling approach for analyses of large interconnected power systems, applied to a 2030 Western Mediterranean case study, Citation: J. Renewable Sustainable Energy 8 (2016) 55501, https://doi.org/10.1063/1.4962415.http://aip.scitation.org/toc/rse/8/5.

[25] G. Wiggins, S. Allu, H. Wang, Battery Cell Data from a 2013 Nissan Leaf, 2020, https://doi.org/10.5281/zenodo.2580327.

[26] I. Dunning, J. Huchette, M. Lubin, JuMP: A Modeling language for mathematical optimization, SIAM Rev. 59 (2) (2017) 295–320, https://doi.org/10.1137/15M1020575.

[27] A. Wächter, L.T. Biegler, On the implementation of an interior-point filter line-search algorithm for large-scale nonlinear programming, Math Program 106 (1) (2006) 25–57, https://doi.org/10.1007/s10107-004-0559-y.

[28] B. Tasseff, C. Coffrin, A. Wächter, C. Laird, Exploring Benefits of Linear Solver Parallelism on Modern Nonlinear Optimization Applications, 2019 arXiv:1909.08104.pdf.

[29] Natural Resources Canada, High-Resolution Solar Radiation Datasets, 2020.https://www.nrcan.gc.ca/energy/renewable-electricity/solar-photovoltaic/18409.